DRAFT VERSION MAY 12, 2020
Preprint typeset using LaTeX style emulateapj v. 01/23/15

# SDSS-IV MANGA: RADIAL PROFILES OF SPECIFIC STAR FORMATION RATE IN NEARBY INTERACTING GALAXIES

JOSHUA L. STEFFEN[1], HAI FU[1], AND MANGA TEAM

*Draft version May 12, 2020*

## ABSTRACT

*Keywords:* galaxies: active — galaxies: nuclei — galaxies: interactions

## 1. INTRODUCTION

In the ΛCDM model, galaxy evolution is a hierarchical process. Over the lifetime of the universe, smaller galaxies have iteratively merged with each other to form more massive galaxies. In fact, cosmological hydrodynamical simulations have shown that repeated merger events may be responsible for as much as ∼60% of stellar mass in massive galaxies like M87 (e.g. Rodriguez-Gomez et al. (2016); Pillepich et al. (2018)).

The internal dynamics of these interacting galaxies were first modeled in the seminal work, Toomre & Toomre (1972). Since then, hydrodynamical simulations have expanded upon the N-body simulations of Toomre & Toomre (1972) by modeling gas-dynamics within the galaxies. These simulations show how barred structures develop within the disks of the interacting galaxies due to the tidal torques between them (Barnes & Hernquist 1991). As the bars form, the gases within the galaxy's disk lose angular momentum and get funneled into the centers of the galaxies.

When the gas-inflows impact upon the gases in the nucleus of galaxy a burst of new star formation in triggered (Barnes & Hernquist 1996; Mihos & Hernquist 1996). These gas inflows will also bring metal-poor gases from the disk into the center of the galaxy which can dilute the central metallicity (Rupke et al. 2010; Perez et al. 2011; Scudder et al. 2012). The gas-inflows may also be able to make it into very center of the galaxy and trigger supermassive black hole (SMBH) accretion (Capelo et al. 2017).

Centrally enhanced star formation has also been observed in large spectroscopic surveys including; CfA2 (Barton et al. 2000; Woods et al. 2006), 2dF (Lambas et al. 2003), AEGIS (Lin et al. 2007), SDSS (Ellison et al. 2008), COSMOS (Kartaltepe et al. 2007; Xu et al. 2012), PRIMUS (Wong et al. 2011), and GAMA (Robotham et al. 2014).

This star formation enhancement increases with closer projected separations between the two galaxies (Ellison et al. 2008; Scudder et al. 2012) but has still shown to be detectable at wide projected separations of 150 kpc (Patton et al. 2013). The level of the star formation enhancement also increases with smaller stellar mass ratios, $|\Delta logM|$, between the two galaxies (Ellison et al. 2008).

With the recent large integral field spectroscopic (IFS) surveys, interacting galaxies can be studied in unprecedented spatial detail. Where previous spectroscopic surveys where limited to the nucleus of the interacting galaxies, the new IFS surveys will be able to study both the nuclei and the disks of the interacting galaxies.

Barrera-Ballesteros et al. (2015) studied star formation in interacting galaxies with the CALIFA[2] survey using variable aperture sizes from which the star formation rate (SFR) is extracted from.

This paper is organized as follows; in Section 2 we will discuss the detail of the MaNGA survey, in Section 3 we will discuss how we extract emission lines from the MaNGA survey and how we calculate the star formation from them, in Section 4 we discuss the construction of our pair sample, in Section 5 we discuss the construction of our control sample, in Section 6 we build the radial profiles for the pair and control galaxies, in Section 7 we discuss the results of the survey, in Section 8 we discuss our results in the context of other surveys, and in Section 9 we summarize and conclude the work.



J.S. and H.F. acknowledge support from the National Science Foundation (NSF) grant AST-1614326 and University of Iowa funds.

## REFERENCES

Baldwin, J. A., Phillips, M. M., & Terlevich, R. 1981, PASP, 93, 5
Barnes, J. E., & Hernquist, L. 1996, ApJ, 471, 115
Barnes, J. E., & Hernquist, L. E. 1991, ApJL, 370, L65
Barrera-Ballesteros, J. K., Sánchez, S. F., García-Lorenzo, B., et al. 2015, A&A, 579, A45
Barton, E. J., Geller, M. J., & Kenyon, S. J. 2000, ApJ, 530, 660
Bundy, K., Bershady, M. A., Law, D. R., et al. 2015, ApJ, 798, 7
Capelo, P. R., Dotti, M., Volonteri, M., et al. 2017, MNRAS, 469, 4437
Chandrasekhar, S. 1943, ApJ, 97, 255
Croom, S. M., Lawrence, J. S., Bland-Hawthorn, J., et al. 2012, MNRAS, 421, 872
Ellison, S. L., Patton, D. R., Simard, L., & McConnachie, A. W. 2008, AJ, 135, 1877
Fu, H., Steffen, J. L., Gross, A. C., et al. 2018, ApJ, 856, 93
Kartaltepe, J. S., Sanders, D. B., Scoville, N. Z., et al. 2007, ApJS, 172, 320
Kewley, L. J., Dopita, M. A., Sutherland, R. S., Heisler, C. A., & Trevena, J. 2001, ApJ, 556, 121

[1] Department of Physics & Astronomy, The University of Iowa, 203 Van Allen Hall, Iowa City, IA 52242

[2] Calar Alto Legacy Integral Field Area

Lambas, D. G., Tissera, P. B., Alonso, M. S., & Coldwell, G. 2003, MNRAS, 346, 1189
Larson, R. B., & Tinsley, B. M. 1978, ApJ, 219, 46
Lin, L., Koo, D. C., Weiner, B. J., et al. 2007, ApJL, 660, L51
Martin, N. F., Ibata, R. A., Bellazzini, M., et al. 2004, MNRAS, 348, 12
Mihos, J. C., & Hernquist, L. 1996, ApJ, 464, 641
Pan, H.-A., Lin, L., Hsieh, B.-C., et al. 2019, ApJ, 881, 119
Patton, D. R., Torrey, P., Ellison, S. L., Mendel, J. T., & Scudder, J. M. 2013, MNRAS, 433, L59
Perez, J., Michel-Dansac, L., & Tissera, P. B. 2011, MNRAS, 417, 580
Pillepich, A., Nelson, D., Hernquist, L., et al. 2018, MNRAS, 475, 648
Robotham, A. S. G., Driver, S. P., Davies, L. J. M., et al. 2014, MNRAS, 444, 3986
Rodriguez-Gomez, V., Pillepich, A., Sales, L. V., et al. 2016, MNRAS, 458, 2371
Rupke, D. S. N., Kewley, L. J., & Chien, L. H. 2010, ApJ, 723, 1255
Sánchez, S. F., Kennicutt, R. C., Gil de Paz, A., et al. 2012, A&A, 538, A8
Scudder, J. M., Ellison, S. L., Torrey, P., Patton, D. R., & Mendel, J. T. 2012, MNRAS, 426, 549
Simard, L., Mendel, J. T., Patton, D. R., Ellison, S. L., & McConnachie, A. W. 2011, ApJS, 196, 11
Thorp, M. D., Ellison, S. L., Simard, L., Sánchez, S. F., & Antonio, B. 2019, MNRAS, 482, L55
Toomre, A., & Toomre, J. 1972, ApJ, 178, 623
White, S. D. M., & Rees, M. J. 1978, MNRAS, 183, 341
Wong, K. C., Blanton, M. R., Burles, S. M., et al. 2011, ApJ, 728, 119
Woods, D. F., Geller, M. J., & Barton, E. J. 2006, AJ, 132, 197
Xu, C. K., Zhao, Y., Scoville, N., et al. 2012, ApJ, 747, 85
Zwicky, F. 1959, Handbuch der Physik, 53, 373

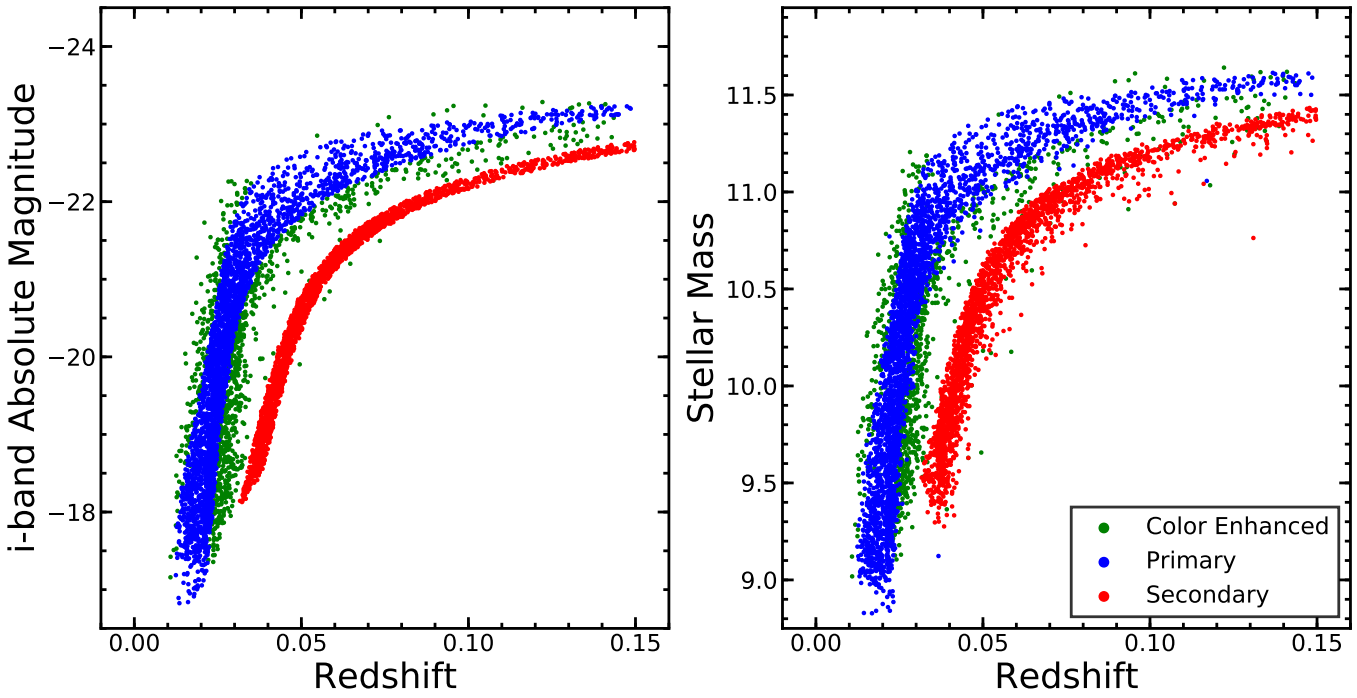


**Figure A1.** On the left is the luminosity - redshift distribution of the MaNGA sample. The figure illustrates the unique distribution of the MaNGA sample. On the right, I replace the luminosity with stellar mass from the NSA catalog.

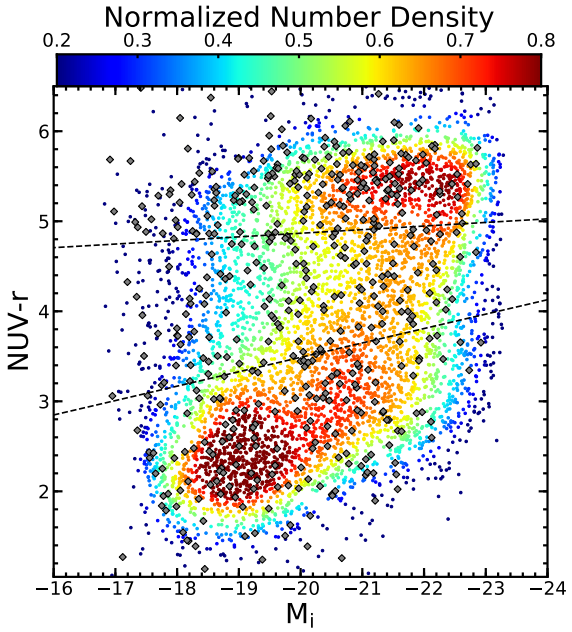


**Figure A2.** Color-magnitude diagram for MaNGA galaxies (*colored circles*). The color of the symbol reflects the local density around each data point in this color-magnitude plane, as indicated by the color bar on the top. The MaNGA galaxies with close companions are marked with *grey diamonds*. From top to bottom, the dashed lines divide the sample into red sequence, green valley, and blue cloud. The star-forming galaxy sample used in this paper are the galaxies below the lower dividing line.

# APPENDIX

## A. FIGURES

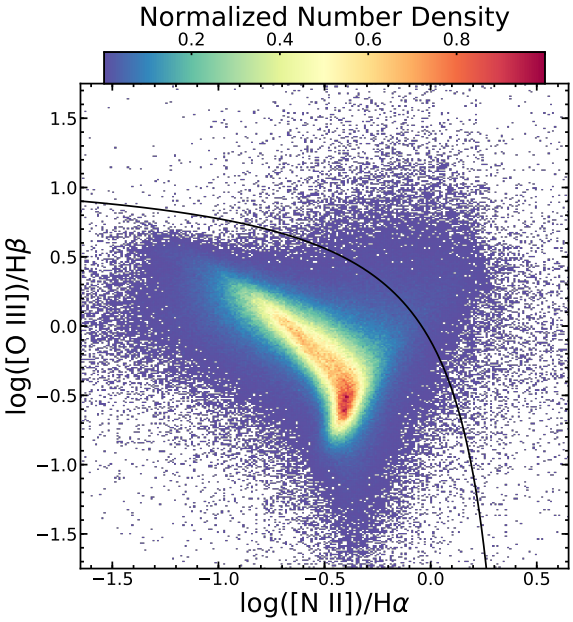


**Figure A3.** The 2-D histogram showing the BPT classification (Baldwin et al. 1981) of individual spaxels within our star-forming control and pair samples. The color of each bin represents the number density of spaxels, normalized to one. The black line represents the theoretically determined maximum starburst line of Kewley et al. (2001). This shows the capability of the CMD to select star-forming galaxies as most of the spaxels within the selected galaxies fall beneath the starburst line.

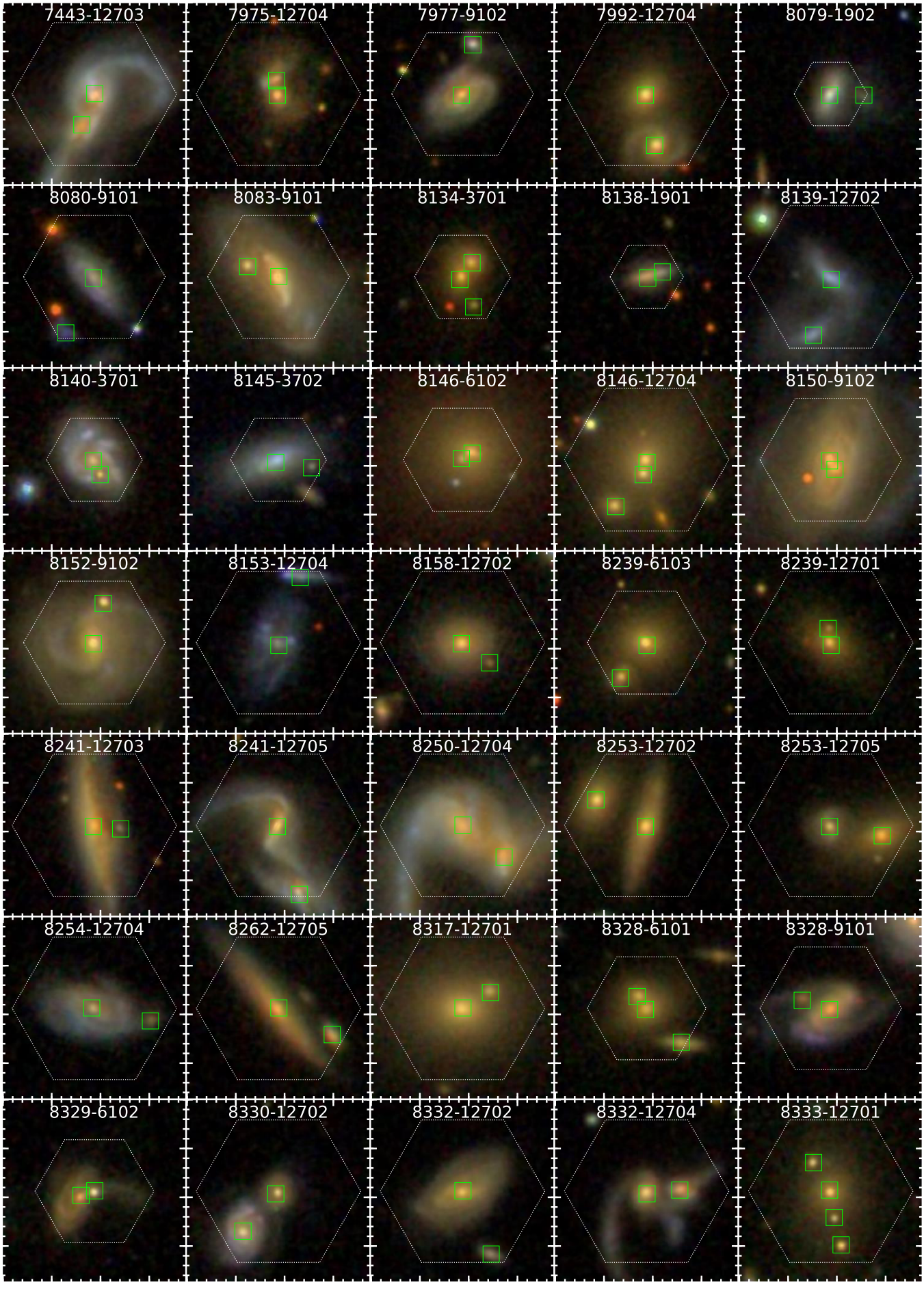


**Figure A4.** A collage of a subset of the inside-IFU pairs. Each panel contains a 40″ cutout of the SDSS pseudocolor image for the galaxy pair. The minor ticks

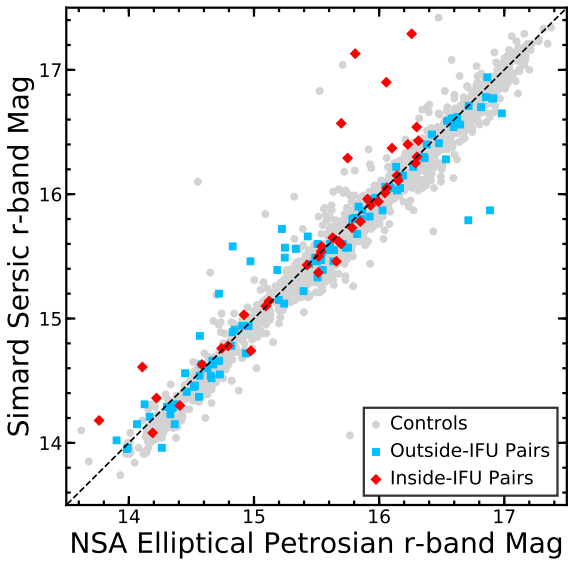


**Figure A5.** The comparison between the Sérsic r-band apparent magnitude in Simard et al. (2011) and the Elliptical Petrosian r-band apparent magnitude. The grey circles represent galaxies in the control sample, the blue squares represent galaxies in the outside-IFU sample, and the red diamonds represent the galaxies in the inside-IFU sample. Regardless of the sample, all of the galaxies covered by both of the catalogs have a similar apparent magnitude calculated from either sample.

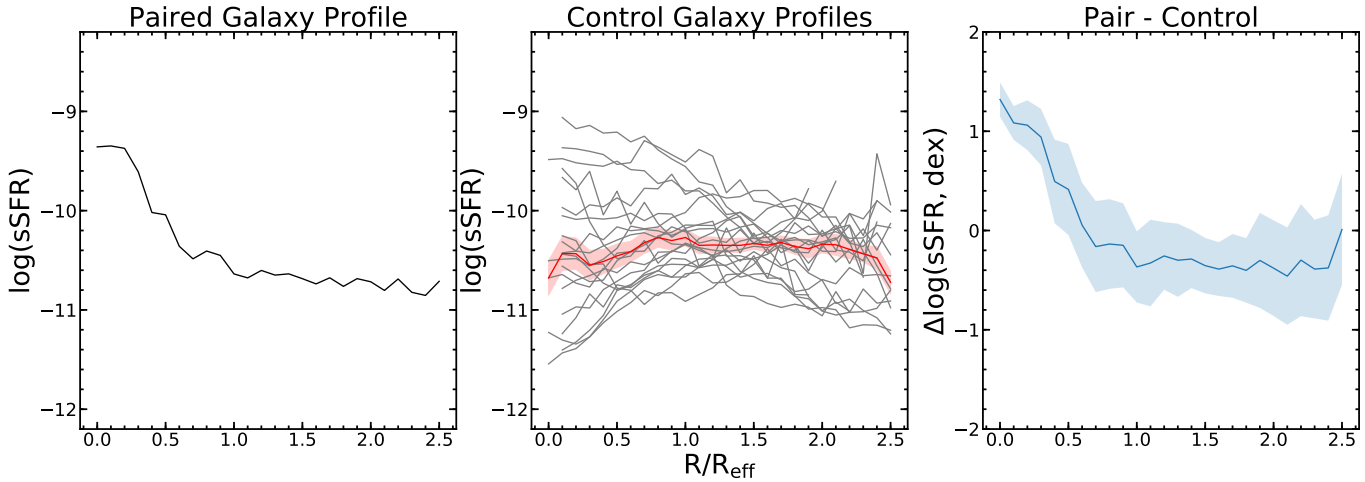


**Figure A6.** The process for building the tailored control sample. The Left panel shows the paired galaxy's profile for sSFR. The Middle panel shows the profiles for sSFR for the selected 20 control galaxies in gray. The red profile is the median profile of the 20 control galaxies where the highlighted region about the profile is the standard error of the mean. The Right panel shows the difference between pair's profile and the stacked control profile.

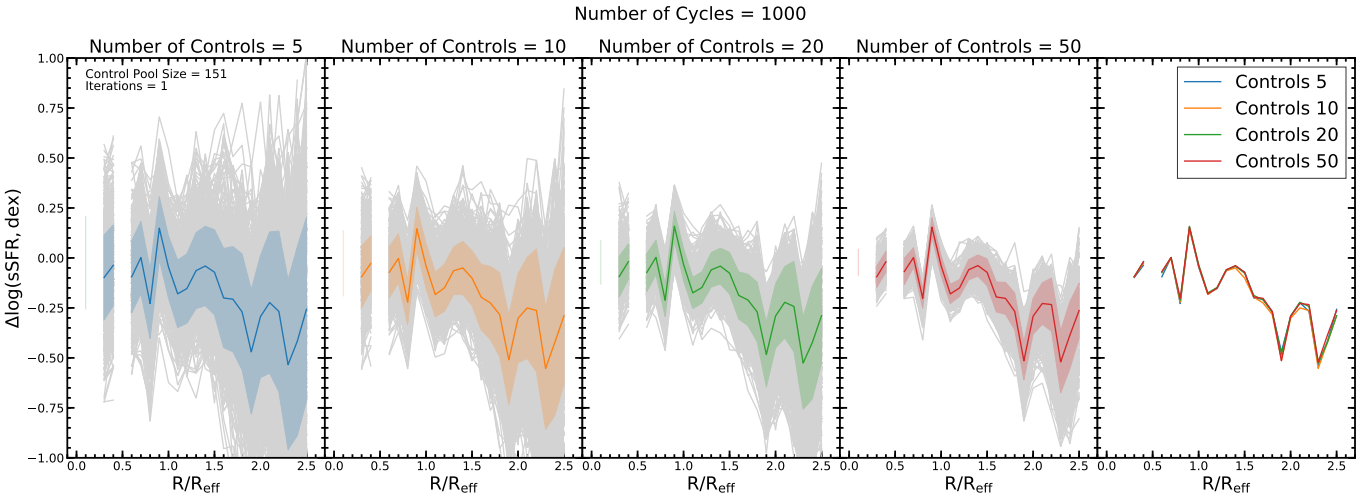


**Figure A7.** An example of the bootstrapping used to quantify the errors associated with the random selection of the control subsample. From left to right, the first four panels show the individual dex profiles after a random sub-selection in grey. The random sub-selection is run 1000 times and the median profile after the 1000 cycles is given by the colored profile. The highlighted region about the colored profiles is the standard error of the mean of the median profile. From left to right each panel shows the random selection for a different number of controls to select; 5, 10, 20, and 50 controls. The panel on the right end shows the median profiles of all of the preceding panels.

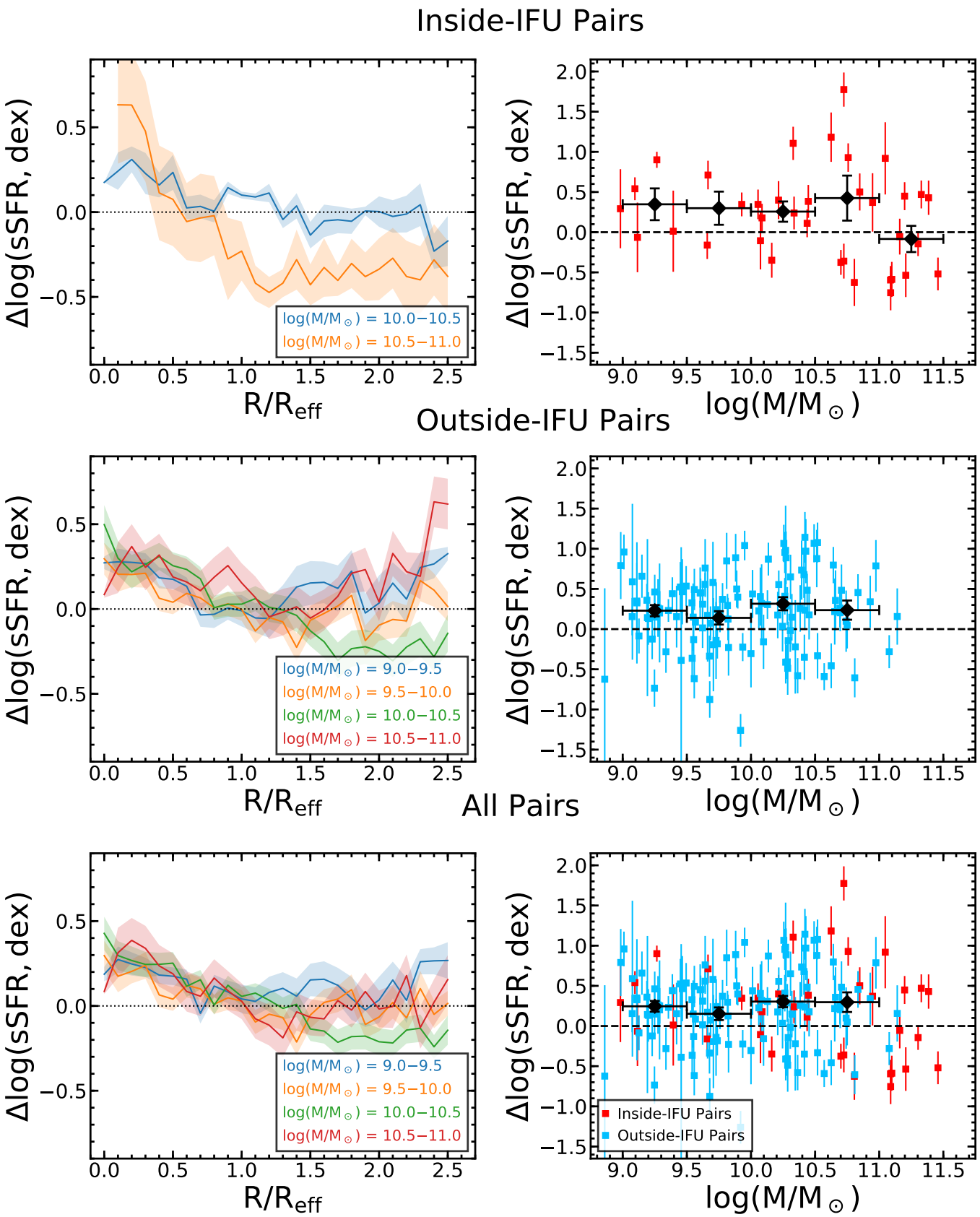


**Figure A8.** The Δlog(sSFR) split into separate stellar mass bins. The left column gives the stacked difference profiles. The highlighted region about the profiles represents the standard error of the mean of the profile. The right column gives the nuclear Δlog(sSFR) values. The black squares are the mean values within a stellar mass bin (where the size of the bins are shown the the horizontal error bars). The vertical error bars on the black squares represent the standard deviation within the bin. The top row is the inside-IFU sample, the middle row is the outside-IFU sample, and the bottom row is the combination of the two samples.

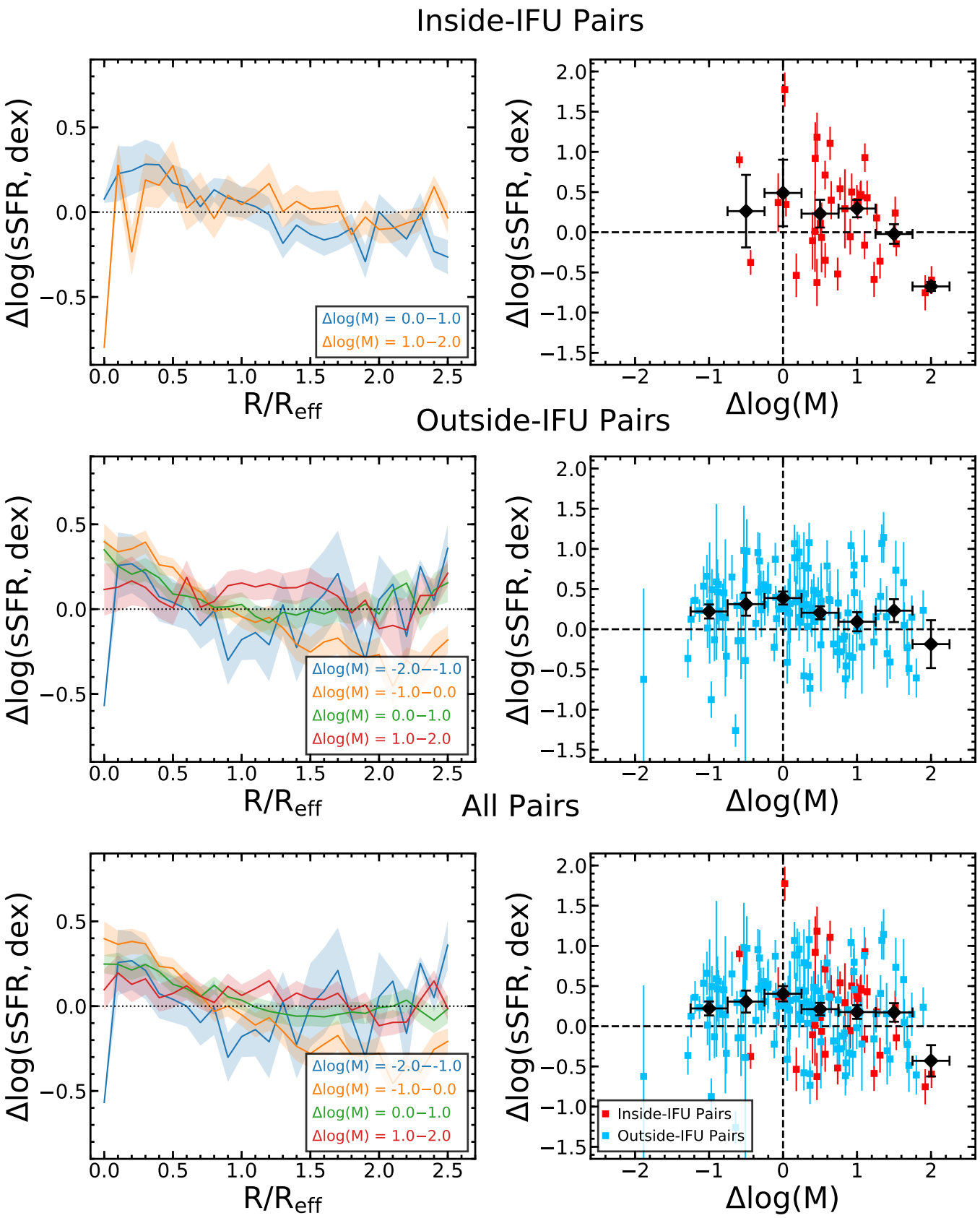


**Figure A9.** Same as Figure A8 but split into separate mass ratio bins.

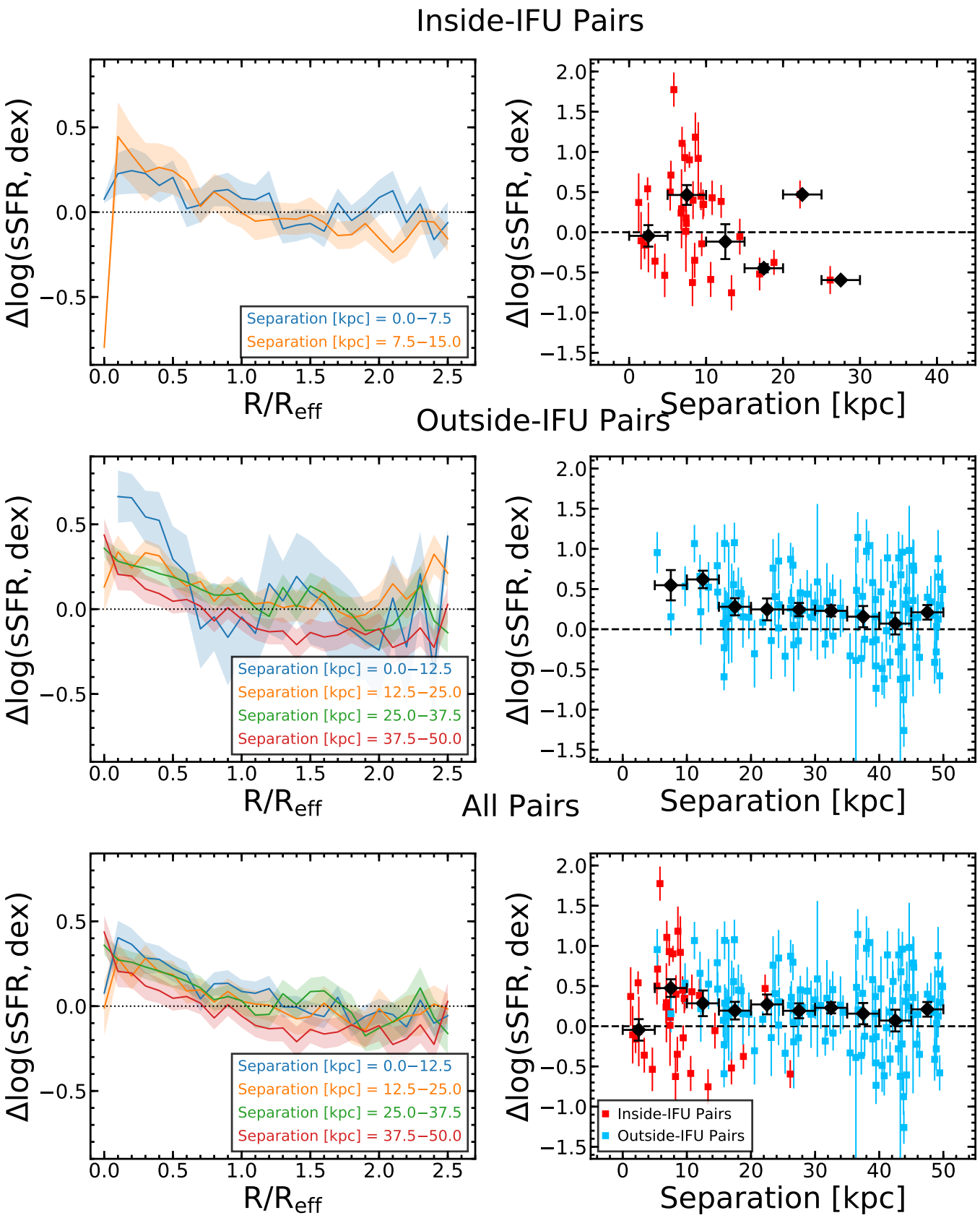


**Figure A10.** Same as Figure A8 but split into separate projected separation bins.

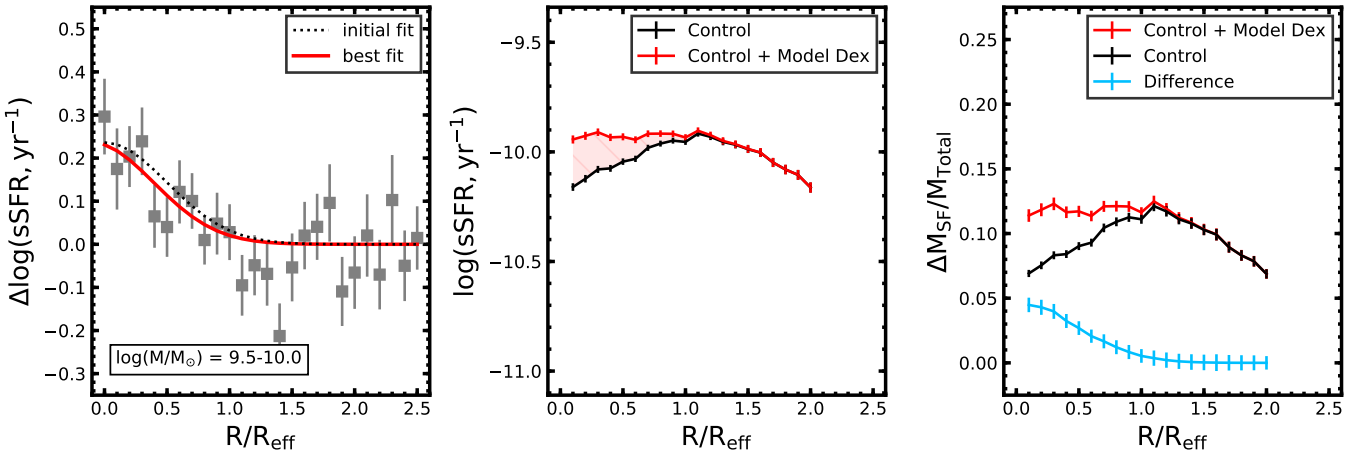


**Figure A11.** In the Left panel we fit a model gaussian to the $\Delta$log(sSFR) profiles. In the Middle panel we plot the log(sSFR) profile for the stacked profiles of the control galaxies (black). We then add the modeled $\Delta$log(sSFR) profile to the control profile (red). The error bars represent the standard error of the mean of the profiles. In the Right panel we show the fractional mass gain due to star formation in the control galaxies (black) and in the paired galaxies (red). The blue profile is the subtraction between the pairs and controls and represents the fractional mass gain due to merger induced star formation. The error bars represent the standard error of the mean of the profiles.

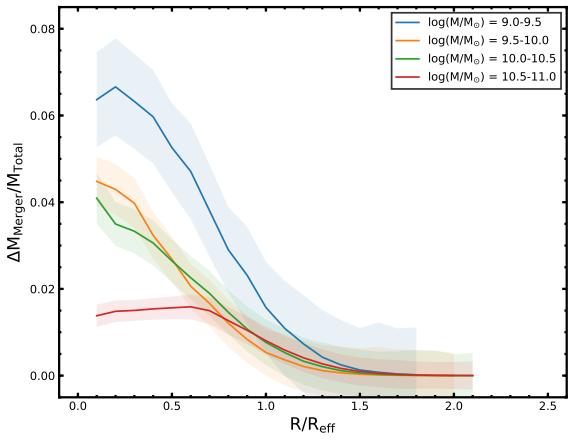


**Figure A12.** The fractional mass gain due to merger induced star formation over a dynamical timescale, $\tau$ = 1 Gyr. The highlighted region represents the propagated standard errors of the mean of the stacked log(sSFR) profiles.